catalysts

MDPI

Article

The Efficiency of Carbon Conversion and Hydrogen Production from Tar Steam Reforming of Biomass Using Ni-Based Catalysts with Alkaline Earth Promoters

Afizah Alir [1,2], Tuan Amran Tuan Abdullah [1,2,*], Anwar Johari [1,2], Mohamed Yusuf Mohamud [1,2], Melissa Low Phey Phey [1,2], Walid Nabgan [3], Francisco Medina [3,*] and Muhammad Ikram [4,*]

1 Centre of Hydrogen Energy, Institute of Future Energy, Universiti Teknologi Malaysia, Skudai 81310, Johor, Malaysia
2 Faculty of Chemical and Energy Engineering, Universiti Teknologi Malaysia, Skudai 81310, Johor, Malaysia
3 Departament d'Enginyeria Química, Universitat Rovira i Virgili, Av. Països Catalans 26, 43007 Tarragona, Spain
4 Solar Cell Applications Research Lab., Department of Physics, Government College University Lahore, Punjab 54000, Pakistan
* Correspondence: tuanamran@utm.my (T.A.T.A.); francesc.medina@urv.cat (F.M.); dr.muhammadikram@gcu.edu.pk (M.I.)

Abstract: H_2 production can be used as a clean and renewable energy source for various applications, including fuel cells, internal combustion engines, and chemical production. Using nickel-based catalysts for steam reforming biomass tar presents challenges related to catalyst deactivation, poisoning, heterogeneous composition, high process temperatures, and gas impurities. To overcome these challenges, adopting a nickel-based catalyst with selected oxide support and MgO and CaO promoter is a promising approach for improving the efficiency and sustainability of steam reforming for hydrogen production. The majority of studies conducted to date have focused on the steam reforming of particular tar compounds, most commonly benzene, phenol, toluene, or naphthalene, over a range of support catalysts. However, the actual biomass tar composition is complex, and each component impacts how well steam reforming works. In this research, a multi-compound biomass tar model including phenol, toluene, naphthalene, and pyrene underwent a steam reforming process. Various types with 10 wt.% of nickel-based catalysts were generated by the co-impregnation technique, which included 90 wt.% different oxide supports (Al_2O_3, La_2O_3, and ZrO_2) and 10 wt.% of combination alkaline oxide earth promoters (MgO and CaO). Thermogravimetric analysis, Brunauer–Emmett–Teller (BET) method, N_2 physisorption, temperature-programmed reduction (H_2-TPR), temperature-programmed desorption (CO_2-TPD), and X-ray diffraction (XRD) of ni-based catalyst characterized physiochemical properties of the prepared catalyst. The reaction temperature used for steam reforming was 800 °C, an S/C ratio of 1, and a GHSV of 13,500 h^{-1}. Ni/La_2O_3/MgO/CaO (NiLaMgCa) produced the most carbon to-gas conversion (86.27 mol%) and H_2 yield (51.58 mol%) after 5 h of reaction compared to other catalysts tested in this study. Additionally, the filamentous carbon coke deposited on the spent catalyst of NiLaMgCa does not impact the catalyst activity. NiLaMgCa was the best catalyst compared to other catalysts investigated, exhibiting a stable and high catalytic performance in the steam reforming of gasified biomass tar. In conclusion, this study presents a novel approach by adding a combination of MgO and CaO promoters to a ni-based catalyst with various oxide supports, strengthening the metal-support interaction and improving the acid-base balance of the catalyst surface. The mesoporous structure and active phase (metallic Ni) were successfully developed. This can lead to an increase in the conversion of tar to H_2 yield gas and a decrease in the production of undesired byproducts, such as CH_4 and CO.

Keywords: nickel; alkaline earth promoter; steam reforming; tar; hydrogen; carbon conversion; CaO; MgO

Citation: Alir, A.; Tuan Abdullah, T.A.; Johari, A.; Mohamud, M.Y.; Phey, M.L.P.; Nabgan, W.; Medina, F.; Ikram, M. The Efficiency of Carbon Conversion and Hydrogen Production from Tar Steam Reforming of Biomass Using Ni-Based Catalysts with Alkaline Earth Promoters. *Catalysts* **2023**, *13*, 472. https://doi.org/10.3390/catal13030472

Academic Editor: Binlin Dou

Received: 12 January 2023
Revised: 19 February 2023
Accepted: 20 February 2023
Published: 23 February 2023

1. Introduction

Limitation supply of fossil fuels promptly and accompanying environmental issues such as global warming and climate change have become global fears. Energy consumption is rapidly growing because of rapid economic development and the expansion of the global population. However, environmental issues about the depletion of fossil resources and large greenhouse gas emissions are growing [1,2], which should be addressed by producing clean and renewable energy. Contamination of the syngas with pollutants, such as tar, ash, compounds containing nitrogen and sulfur, and particularly tar, is entirely intolerable [3]. Tar is a complex mixture of chain hydrocarbons, aromatic hydrocarbons, and heterocyclic organic material. It is a complex mixture of oxygenated and condensable aromatic HCs that condenses at low temperatures, causing issues with the process [4]. For instance, filter clogging, equipment clogging downstream, and coke deposition on the catalyst downstream. In addition, tar contains amounts of polycyclic aromatic hydrocarbons, which are dangerous to human health and pollute the environment. These compounds include phenol, aldehydes, and formaldehyde [5–8]. For converting HCs into H_2-rich gas, the removal of tar by steam reforming is a promising technology [9]. Steam reforming is said to have a higher H_2 output [10,11]. It is the most advanced and attractive method available that offers a conversion mechanism for liquid HCs.

Natural biomass tar has a complex composition. Each of its components affects how well the steam reforming performs. Many recent analysis studies focus on steam reforming using one or two tar model compounds, often phenol, benzene, toluene, or naphthalene, in conjunction with utilizing different supporting metal catalysts [12]. A previous study has attempted to determine how the feedstock's composition affects the catalytic performance during steam reforming. According to their findings, compared to individual feed chemicals, the mixture of toluene and naphthalene affected the catalytic activity and decreased feed conversion [13–16]. Thus, this opens a new research dimension to focus on the mixture of major tar components.

The availability of catalysts that provide a more effective steam reforming has led to the development of numerous catalysts. Thus, obtaining a catalyst with excellent stability that is both selective for H_2 and resistant to coke deposition is incredibly challenging. [17,18]. Ni-based catalysts have been widely utilized in steam reforming, although the creation of coke can deactivate their active sites [17,19]. The catalyst's support is also a crucial component. Support influences the dispersion of active metal particles and the catalytic reaction. Yet, the crucial support material considerations for good catalyst formation are pore structure, acidity-basicity, and metal support interaction. However, some supports, such as Al_3O_2, encourage the formation of coke. Moreover, the high operating temperatures used in biomass gasification may cause the support to collapse or result in the formation of bigger metal clusters, which promotes sintering due to a loss in metal dispersion. Hence, catalyst supports are modified with promoters to lessen some of these effects for better tar reforming catalyst performance, or by lowering the reaction temperature [20]. In this study, Ni-based catalysts were supported with three different types of supports, including lanthanum oxide (La_2O_3), alumina (Al_2O_3), and zirconia (ZrO_2). These oxides are thermally stable, can withstand the high temperatures required for steam reforming reactions, and have a high surface area, which helps to increase the number of active sites available for catalytic reactions. A previous study showed that Al_2O_3 and La_2O_3 supported catalysts to produce a low level of CH_4 gas due to their excellent ability to reform produced CH_4. Even though nickel-based catalysts with La_2O_3 support have a small BET surface area, the basicity of it was essential to promote the catalytic activity in steam reforming [21]. Studies regarding the nickel-based catalyst supported by ZrO_2 illustrate that large pore size improved bio-oil bulky molecule accessibility to Ni sites, resulting in enhanced catalytic activity [22]. According to recent findings, adding alkaline earth metal oxides such as MgO and CaO as a promoter could lessen the catalyst's acidity, improve the steam-carbon reaction, and favor H_2O adsorption and OH mobility on the surface. These effects, in turn, boost the coke suppression rate and catalytic stability [16,23,24].

The presence of alkaline earth metal oxides could enhance the activation of the main hydroxyl group and C-H bond, resulting in good catalytic performance, according to reaction kinetics from a prior study [25]. Additionally, it favors H_2 generation by adsorbing CO_2, which causes the reaction of WGS thermodynamic equilibrium to shift in favor of H_2 production [26,27]. The MgO addition to Ni/Al_2O_3 is responsible for the catalyst's sintering resistance property, according to a previous study by Nogueira et al. This property allows the catalyst to produce stable steam reforming of acetic acid with 91% conversion for a 24 h reaction time at 600 °C catalyst temperature. $MgAl_2O_4$ is produced when MgO is present, which prevents the creation of coke [28]. According to a study by Baidya et al., complete conversion of toluene was achieved at 800 °C with the combination of the promoting effects of both CaO and CeO_2 on the surface of Ni/CARBO HSP support, and the conversion rate only decreased by 7% after 48 h of reaction time [29]. CaO is a stronger promoter with higher basicity, which can enhance the catalytic activity and selectivity of a catalyst. However, CaO is also more prone to sintering and deactivation, and is more susceptible to poisoning by impurities in the feedstock. In contrast, MgO is typically more stable and less expensive, making it a more appealing choice for high-temperature and prolonged catalytic processes. MgO is also less likely to form compounds with impurities in the feedstock, which can improve the longevity and activity of the catalyst. In this study, combination of both MgO and CaO as promoters of modified catalyst insteam reforming of the multi-compound biomass tar model was investigated to see the performance of the catalyst H_2 yield, carbon conversion percentage as well as coke formation in spent catalyst.

This work aims further to improve the catalytic activity of the ni-based catalyst. Therefore, we prepare a series of catalysts modified by various oxide support (Al_2O_3, ZrO_2, and La_2O_3) and a combination of alkaline oxide earth (MgO and CaO) and deeply investigate the effect of promoters on catalytic performance under the mixture of biomass tar steam reforming process. Finally, the stability of the catalytic performance of modified catalysts with improved activity and coke formation was assessed.

2. Results and Discussion

2.1. Catalyst Characterization

All TGA was used to assess the thermal stability of the catalyst. As seen in Figure 1, multiple stages of decomposition were demonstrated by a ni-based catalyst. The subsequent pathway offers an explanation for this, including; the dehydration of intermediate-type nickel nitrate (II) hydrate ($Ni(NO_3)_2 \cdot xH_2O$), denitration of nickel nitrate ($Ni(NO_3)_2$), decomposition of nickel (Ni_2O_3) and finally the formation of nickel oxide (NiO). The weight loss observed was categorized into two stages: below 200 °C and above 200 °C, as listed in Table 1. The initial weight loss happened below 200 °C caused by thermal dehydration of physically absorbed water and volatile contaminants throughout the synthesis pathway. The weight loss of catalyst above 200 °C occurred from the conversion of amorphous to crystalline phase such as nickel nitrate hexahydrate to nickel oxide (NiO). Figure 1 also shows that the zero weight changes are seen at temperatures more than 750 °C, suggesting that the catalysts were fully decomposed. Catalysts must be calcined at an optimum calcination temperature of 750 °C to allow for complete nickel oxide phase formation and the catalyst's structure and textural properties. Results also show that catalysts with promoters have a more significant weight loss than those without promoters. The addition of MgO and CaO promoters also has some drawbacks. The high-temperature operation of the catalyst can lead to increased sintering, resulting in higher weight loss in TGA analysis. This can be due to the sintering of the active Ni species and the formation of larger, less active particles. In contrast, Ni-based catalysts with La_2O_3, ZrO_2, and Al_2O_3 support without promoters may have lower weight loss due to their lower sintering rate and smaller active surface area. This can result in a longer catalyst lifetime and lower catalytic activity than catalysts with MgO and CaO promoters.

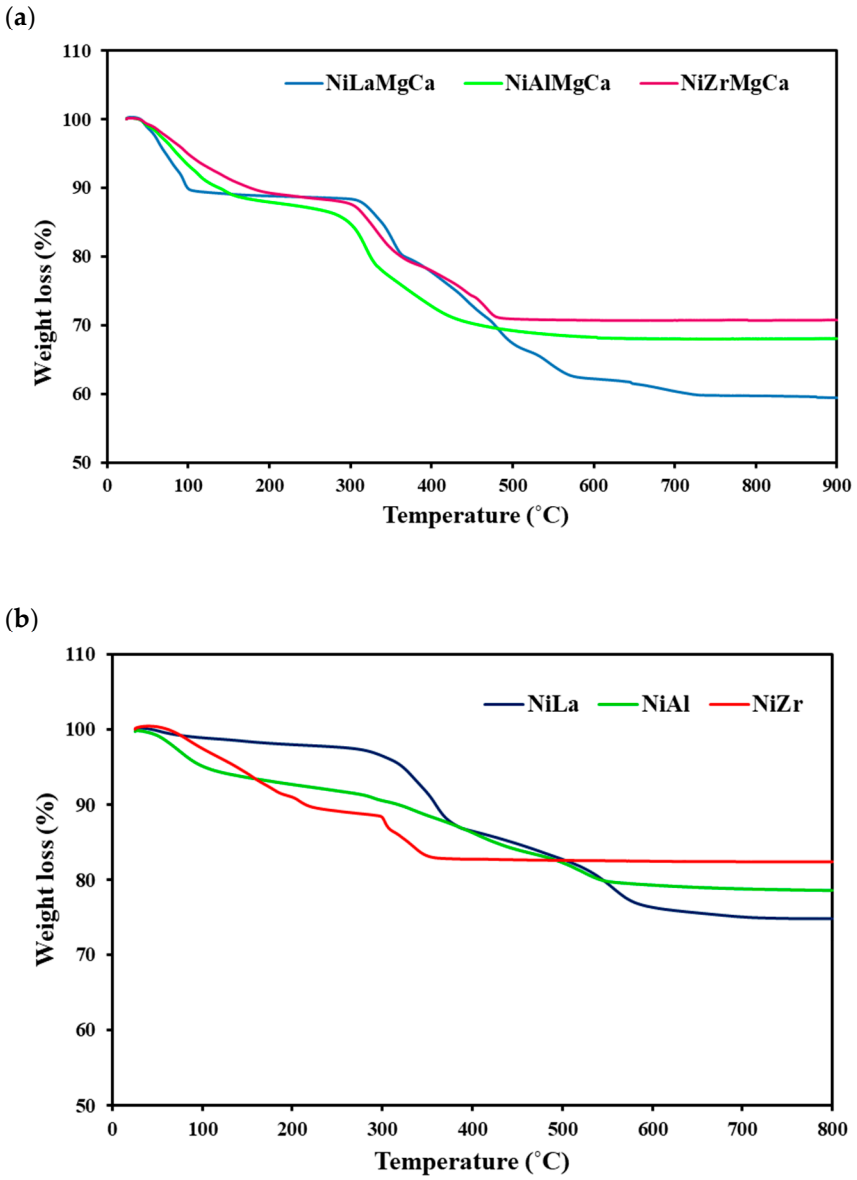

Figure 1. (**a**) TGA graph of fresh Ni-based catalyst with MgO and CaO promoter; (**b**) TGA graph of fresh Ni-based catalyst without MgO and CaO promoter.

Table 1. Weight loss (%) of fresh catalyst by TGA.

Catalyst	Weight Loss (%)		Overall Weight Loss (%)
	Below 200 °C	Above 200 °C	
NiLa	2.02	23.11	25.13
NiZr	8.71	16.16	24.87
NiAl	6.93	14.17	21.10
NiLaMgCa	11.19	29.39	40.57
NiZrMgCa	10.55	18.70	29.25
NiAlMgCa	12.06	19.88	31.94

H_2-TPR was then used to describe the reducibility of the calcined catalysts. The findings demonstrated that the catalysts had multiple-stage reduction between 300 and 1000 °C due to varying degrees of reducible metal oxide-support interaction. As reported by other researchers, it is interesting to notice that the reduction peak in the H_2-TPR study shifts toward a higher temperature range with adding MgO and CaO promoters [30].

Figure 2 illustrates the TPR profiles for a specific temperature range. The free-state NiO particle (phase I; <300 °C) is the easiest to reduce based on reduction efficiency [31,32], followed by the bulk NiO particle that decreases in contact area (phase II; 300–450 °C) [33] and followed by the next stage (phase III; 450–600 °C) which was NiO reduction that had substantial interaction with the support [34,35]. Finally, solid solution (NiO-MgO and NiO-CaO) [36,37] and spinel type NiO (spinal made of $NiLa_2O_4$) [34,38,39] are the most difficult to reduce (phase IV; >600 °C). With the significant peak measured at 645 °C, the NiLaMgCa catalyst had the highest reduction temperature among catalysts. The reduction of non-stoichiometric spinel-type metals is responsible for these findings. It is possible that the promoter species covering the Ni surface prevents the catalyst from being reduced, causing the reduction temperature to rise at higher metal compositions [40]. As a result, the promoter's composition accounts for the more prominent peak at this temperature range than other catalysts [41]. The NiLaMgCa catalyst demonstrated free NiO's presence and suggested that until the maximum structural limit was reached in the low-temperature region, the gradual oxygen loss could be correlated with H_2 consumption (phase II) [42]. NiOx is typically only partially reduced to metallic Ni at lower reduction temperatures, whereas metallic Ni agglomeration causes the catalyst to deactivate at higher temperatures. Thus, the reduction temperature used in this investigation for all catalysts was 750 °C.

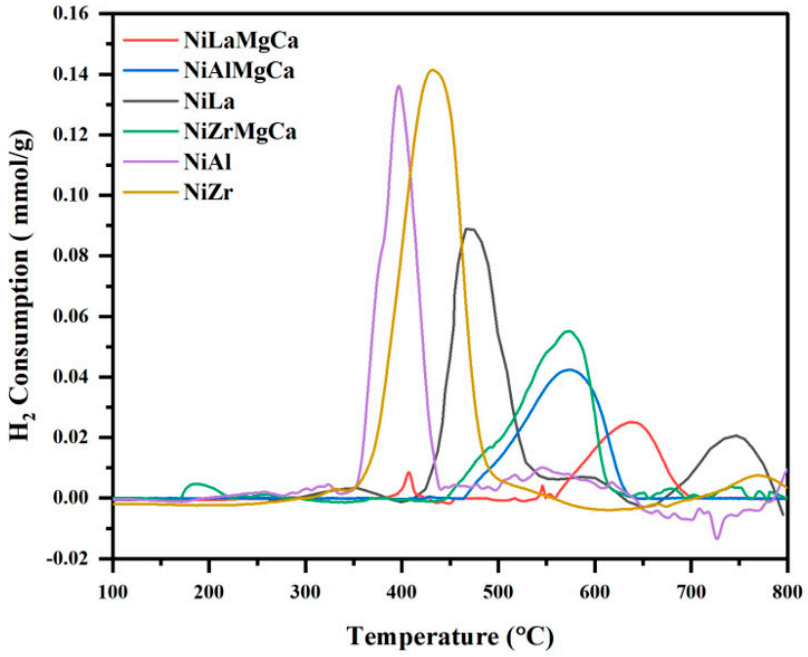

Figure 2. H_2-TPR profiles of the calcined catalyst.

Figure 3 illustrate the crystalline phase of the ni-based catalyst modified with support and promoters. To determine the catalytic activity during the steam reforming of gasified biomass tar; it is shown that selecting the right support material was more critical than textural aspects. As shown in Table 2, the XRD analysis determined that Ni crystalline and Ni dispersion sizes were 27.64–53.11 nm and 1.9–2.68%, respectively. The presence of $NiAl_2O_4$ on the NiAlMgCa catalyst at $2\theta = 32.1^\circ$ and 39.5°, as shown in XRD profiles, indicates that NiO interacted with Al_2O_3 to produce the spinel during calcination and that it cannot be reduced entirely at 900 °C. Additionally, the NiLaMgCa and NiZrMgCa catalysts did not exhibit any CaO characteristic peaks, indicating that CaO is either well dispersed or is present as an amorphous structure in these catalysts [23,43,44]. For NiZrMgCa catalysts, the hydroxylation of water humidity during handling and storage has formed the portlandite phase, notably $Ca(OH)_2$. Due to the hygroscopic nature of the La_2O_3 support, lanthanum hydroxide ($La(OH)_3$) was expected to emerge in NiLaMgCa [23].

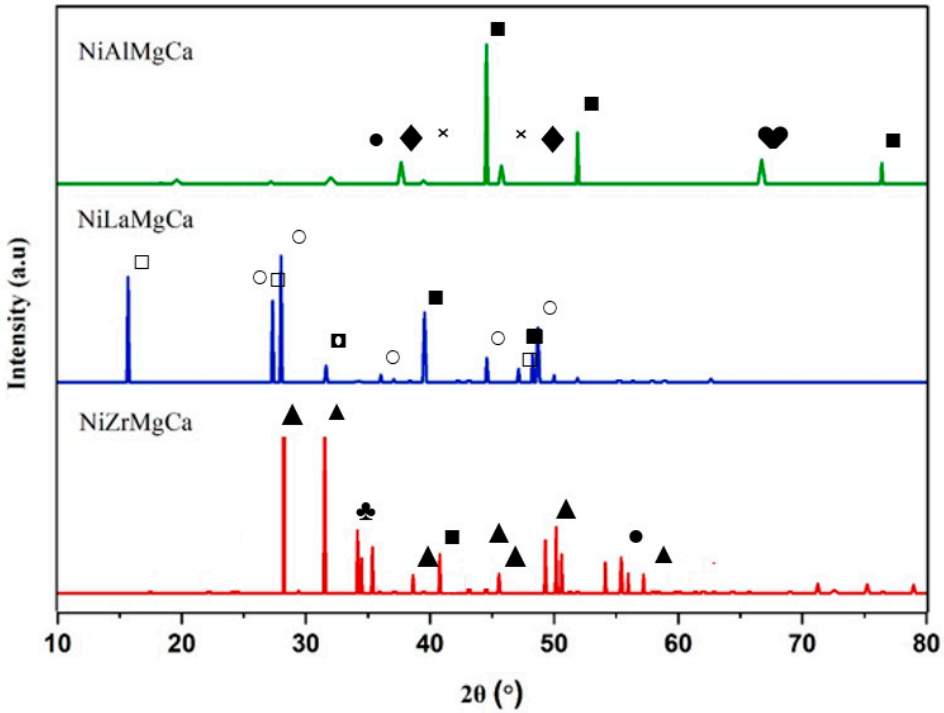

Figure 3. Crystalline phase of XRD profile reduced catalyst; Ni (■); MgO (●); CaO (♥); $Ca(OH)_2$ (♣); Al_2O_3 (▲); $NiAl_2O_4$ (×); La_2O_3 (○); La $(OH)_3$ (□); $NiLa_2O_4$ (◘); ZrO_2 (▲).

To sustain the catalytic activity, the adsorption of CO_2 on the catalyst surface is also crucial, and different NiO content shows various basicity strengths [45,46]. CO_2-TPD analysis was conducted to quantify the basic sites of the modified catalysts shown in Figure 4. Interaction between the basic sites and CO_2 is revealed by the correlation between the strength of the basic sites and the peak position [47]. As shown in Figure 4, weak and strong basic strength desorption is associated with temperatures below 250 °C and above 400 °C. It is observed that for catalyst NiAlMgCa desorbed CO_2 at 488 °C and 747 °C, attributed mainly to the weak basic sites. NiAlMgCa catalyst shows that doping Al_2O_3 with base metal oxides (MgO and CaO) as a promoter suppresses or neutralizes the Lewis acidic centers, which helps activate the C-H bond in tar hydrocarbons compared to the NiAl catalyst that shows no based sites [45,46]. The NiZrMgCa catalyst indicated that the CO_2 desorption peak was at 691 °C. NiZrMgCa shows a basicity peak at a high temperature, which suggests that the basic sites on the catalyst surface are thermally stable and persist at high temperatures compared with NiZr, which typically shows no basicity peak. NiLaMgCa catalyst showed a broad asymmetric desorption peak at 474 °C, extending to 747 °C. In comparison, the NiLa catalyst only showed a peak at 455 °C because no addition of MgO and CaO promoter contributes less basicity in the catalyst. The order of the catalyst's total number of basic sites was NiLaMgCa > NiZrMgCa > NiAlMgCa > NiLa > NiZr > NiAl. The addition of MgO and CaO as promoters increased the basicity sited of the catalyst compared to those without a promoter, as reported in the previous study [24,34,48–52]. The result suggested that higher basicity likely contributes to high catalytic performance by enhancing steam coke reaction, suppressing coke formation, improving tar conversion, higher hydrogen yields, and lower carbon monoxide production in steam reforming processes. When MgO and CaO were added as promoters to a nickel-based catalyst, they can modify the nickel surface properties and catalyst surface basicity of nickel. This can result in stronger adsorption of CO_2 molecules on the catalyst surface and higher activation energy required for the desorption of CO_2. As a result, more energy is needed to heat the catalyst to a temperature at which CO_2 desorption occurs, and this desorption temperature shifts to a higher temperature. This result demonstrates that catalysts with alkaline earth

promoters exhibit superior catalytic activity for H_2 production compared to catalysts that only utilize oxide supports.

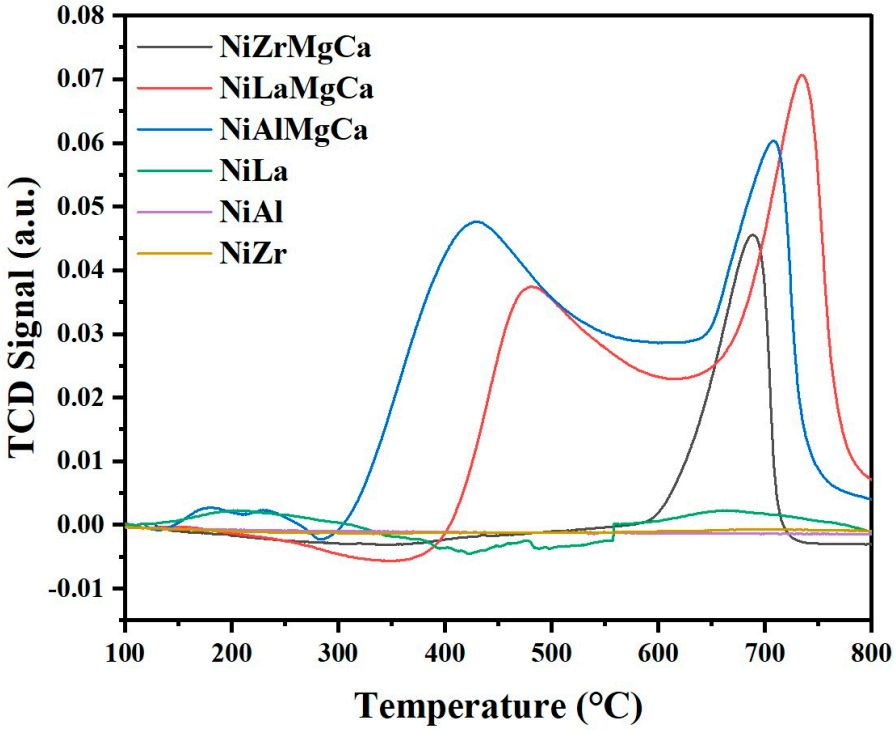

Figure 4. CO_2–TPD profiles of reduced catalyst.

Textural characteristics of reduced catalyst were analyzed using N_2 physisorption isotherms as presented in Table 1. Compared to other reduced catalysts, the NiAlMgCa catalyst had the largest. Catalyst with Al_2O_3 support shows a larger BET surface area than other supports material. In comparison, this catalyst, with adding of MgO and CaO, had a smaller BET surface area (68.57 m^2/g) and pore volume (0.23 cm^3/g) compared to the catalyst without the promoter, which was BET surface area (92.95 m^2/g) and pore volume (0.27 cm^3/g). Adding MgO and CaO to a nickel-based catalyst can lead to a lower BET surface area but probably have better catalytic activity. This is because the promoter can modify the structure and composition of the active sites, leading to the formation of more active nickel species, thus increasing the catalytic activity. In addition, the promoter can also increase nickel dispersion on the Al_2O_3 support, leading to a more uniform distribution of active sites, consequently improving the catalytic activity. Furthermore, the BET surface area of catalysts increased in the order of NiZr < NiLa < NiAl < NiZrMgCa < NiLaMgCa < NiAlMgCa. Figure 5 illustrates the reduced catalyst's Brunauer-Joyner-Halenda (BJH) pore size. NiAlMgCa probably has greater catalytic characteristics about the specific surface area. This is because a larger surface area increases the probability of a collision between the reactants in contact with the catalyst surface; Carb structures with pores that range in size from 2 nm to 50 nm. Every catalyst analysis in this study provided evidence that the mesopore structures were successfully developed. A mesoporous structure that forms on the catalyst during the steam reforming reaction considerably impacts the reactant and heat diffusion. In addition, good resistance to coke formation and Ni sintering large surface areas of mesoporous catalysts can also make them more efficient at adsorbing and desorbing reactants and products, which can improve the selectivity of the catalytic reaction [53,54].

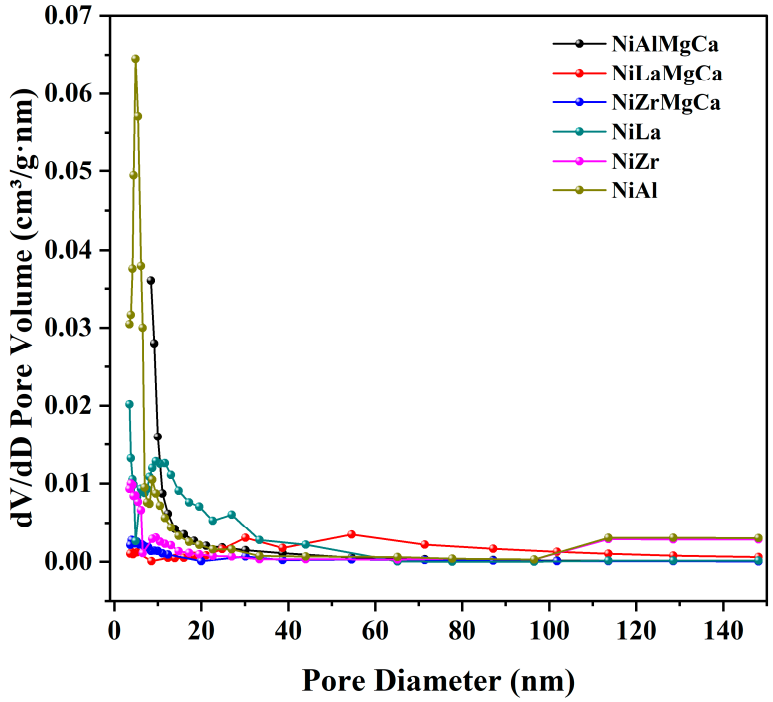

Figure 5. BJH pore size of the reduced catalyst.

Table 2. Summary of characterization finding in this study.

Catalyst	BET Surface Area (m^2/g) [1]	Pore Volume (cm^3/g) [2]	Average Pore Size (nm) [3]	Ni crystallite Size (nm) [4]	Ni Dispersion (%) [5]
NiLaMgCa	15.80	0.184	46.57	37.64	2.68
NiAlMgCa	68.57	0.23	13.42	39.46	2.56
NiZrMgCa	5.48	0.035	25.51	53.11	1.90
NiLa	28.85	0.16	22.18	-	-
NiAl	92.95	0.27	11.62	-	-
NiZr	9.79	0.082	33.65	-	-

[1] Determined by ρ/ρo of 0.05–0.30 using BET equation by assuming the N_2 molecule cross-sectional area of 0.162 nm^2. [2] Determined at the highest ρ/ρo of 0.99. [3] Pore size = (4000 × pore volume)/BET surface area [23]. [4] Calculated from Ni (111) at 2θ = 44.5° by the Scherrer equation, crystallite size = 0.89λ/βcosθ. [5] Dispersion = 101/crystallite size, assuming that Ni particles exhibit a spherical geometry.

2.2. Catalytic Activity

Figure 6 provides the average values of total gas production, carbon conversion to gas, and H_2 yield for different catalysts throughout the 5 h steam reforming duration of tar model compounds produced via biomass gasification. The following is a ranking of the catalytic performance during carbon gasification; NiLaMgCa > NiZrMgCa > NiAlMgCa. Nevertheless, the order of the H_2 yield for each catalyst was NiLaMgCa > NiAlMgCa > NiZrMgCa. Despite having a small surface area (15.80 m^2/g) and pore volume (0.184 cm^3/g), the NiLaMgCa catalyst produced total gas production (96.67 $mmol/mL_{tar}$), had the highest carbon to gas conversion (86.27%), and had the highest H_2 yield (51.58%) of all the catalysts tested. It is shown that while steam reforming gasified biomass tar, selecting the suitable support and promoter material has a more significant impact on the catalytic activity than textural aspects [21,55]. Table 3 shows the previous study regarding the catalytic steam reforming of tar and its catalytic performance. Nickel-based catalysts supported with La_2O_3, Al_2O_3, and ZrO_2 can effectively catalyze the steam reforming of biomass tar, producing high H_2 yields and having good catalytic activity. These catalysts are also known for their thermal and chemical stability and resistance to poisoning and sintering, which improves the durability of the catalyst.

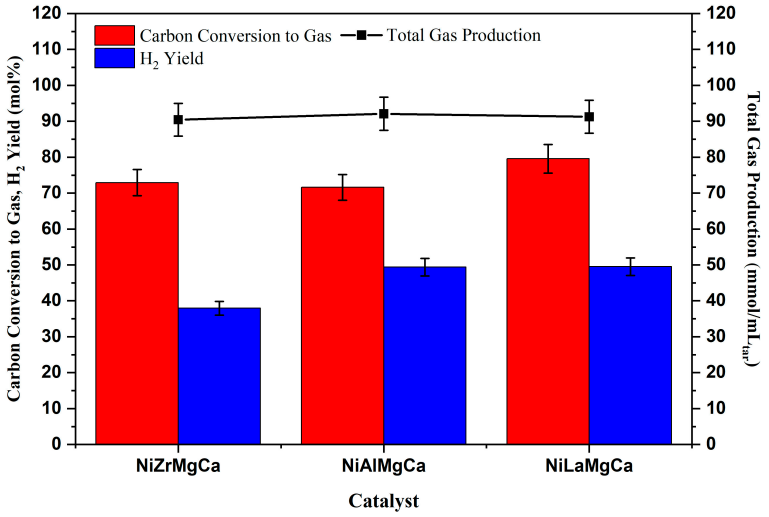

Figure 6. Carbon conversion to gas, H_2 yield, and total gas production from biomass module tar steam reforming over Ni-based catalyst (reaction condition: temperature = 800 °C; S/C ratio = 1; GHSV = 13,500 h^{-1}).

Table 3. Previous studies of Ni-based catalyst tar steam reforming of biomass and the catalytic performance.

Catalyst	Condition	Catalytic Performance	Ref.
Ni/dolomite, Ni/dolomite/Al_2O_3, Ni/dolomite/La_2O_3, Ni/dolomite/CeO_2, Ni/dolomite/ZrO_2	Toluene/pyrene/naphthalene/phenol Temperature = 700 °C; S/C molar ratio = 1	Carbon conversion = 58.84–77.6% H_2 yield = 55.44–66.20%	[23]
Ni/ CHA-t, Ni/Al_2O_3, Ni/SiO_2	Toluene Temperature = 650–800 °C; S/C = 2	H_2 yield = 48–52%	[56]
Ni/Al_2O_3	Phenol, toluene, indene, furfural, methylnaphthalene Temperature = 750 °C; S/C = 2	Carbon conversion = 63–75% H_2 yield = 8–12%	[48]
Ni/ZrO_2, Ni/Co/ZrO_2	Phenol Temperature = 600 °C; S/C = 1.7	H_2 yield = 25–50%	[57]

Figure 7 represents the average selectivity toward the gaseous product and the H_2/CO molar ratio of the reformate made by steam-reforming gasified biomass tar over 5 h over various catalysts. The major gaseous products, as seen, were H_2 (37.6–37.7 mol%) and CO (49.34–49.4 mol%) followed by CO_2 (10.2–10.3 mol%) and CH_4 (2.8–2.83 mol%). According to the findings, steam reforming and the WGS reaction constitute the main reactions in the process. [20,53,58]. CH_4 also showed that only a small amount could be detected because it was further converted into H_2 and CO during the methane steam reforming [23,59]. Additionally, all catalysts in this study showed a lower H_2/CO molar ratio (0.762–0.763) than the stoichiometry value. The gas may undergo incomplete conversion, and catalysts may not be able to convert all of the biomass tar into syngas, resulting in a lower H_2/CO molar ratio. Syngas with a low H_2/CO ratio can be used as feedstock to produce chemicals such as ethanol [60]. To enhance the H_2/CO ratio, modifications can be made to the steam reforming process, such as expanding the steam-to-biomass ratio (S/C ratio). [61–63]. The CO_2 constituent of reformate (10.2–10.3 mol%) produced in this work is slightly low, as described in the literature, which ranges from 10% to 25% according to other researchers [51,64,65].

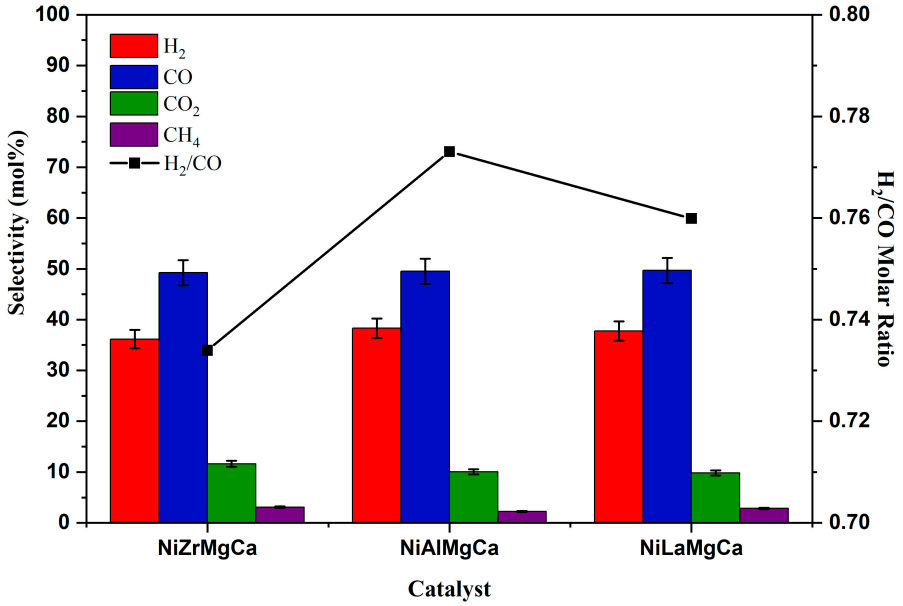

Figure 7. Selectivity of the gaseous products and the H_2/CO molar ratio from the biomass module tar steam reforming over Ni-based catalyst (reaction condition: temperature = 800 °C; S/C ratio = 1; GHSV = 13,500 h^{-1}).

Figure 8 illustrates how the amount of carbon converted to gas and H_2 generated varies over time. Over the time of the 300 min of reaction, various patterns were seen for all catalysts in the production of H_2 and the conversion of carbon to gas: (i) relative consistency over NiLaMgCa and NiAlMgCa for the hydrogen yield, (ii) inconsistent trend of carbon conversion to gas for NiAlMgCa and NiZrMgCa, (iii) slightly increased trend over NiLaMgCa of carbon conversion to gas. ZrO_2 support in NiZrMgCa can be highly reactive with steam injected into the reactor continuously, leading to instability under reaction conditions. It caused the trend for carbon conversion and hydrogen yield to be inconsistent over time. The catalyst of NiLaMgCa is known for its high thermal stability and low diffusion coefficient for carbon, which can help maintain the catalyst's stability during the carbon conversion reaction and reduce carbon accumulation over time. Additionally, La_2O_3 can also help to improve the dispersion of the Ni particles on the support and has a lower tendency to promote the sintering of the Ni particles than Al_2O_3.

(a) (b)

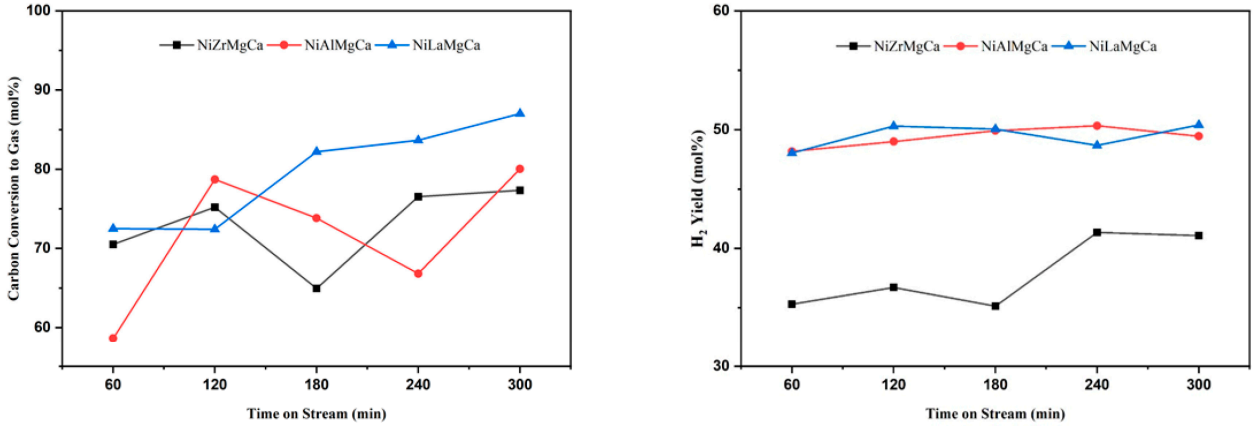

Figure 8. (**a**) Carbon conversion to gas for 5 h experiment; (**b**) hydrogen yield production for 5 h experiment (reaction condition: temperature = 800 °C; S/C ratio = 1; GHSV = 13,500 h^{-1}).

2.3. Characterization Spent Catalyst

Following the 5 h catalytic activity test, each coking resistance of the catalyst and the characteristics of the coke deposited on it were examined using TGA (in the air), as shown in Figure 9. The catalyst weight loss is related to the oxidation of the deposited coke during the TG analysis. Coke deposited on the catalyst surface falls into two categories: amorphous carbons, which were oxidized below 550 °C, and filamentous carbons, which were oxidized between 550–750 °C [23]. According to published research, amorphous carbon deactivates the catalyst, but filamentous carbon has little effect on deactivation but causes reactor blockage and pressure drop [18]. All utilized catalysts, except for the NiAlMgCa catalyst, showed a weight increase in the area of amorphous coke. This could be as a result of (i) the oxidation of metallic Ni particles to produce NiO species, (ii) La_2O_3 and CO_2 react to generate $La_2O_2CO_3$ in a chemical reaction, and (iii) carbonation of CaO results in the production of $CaCO_3$. According to Figure 9, the weight obtained by synthesizing $CaCO_3$ in the area of amorphous carbon is beneficial.

Figure 9 shows that only the region of filamentous carbon experiences weight loss from using the NiLaMgCa catalyst. Additionally, the NiLaMgCa catalyst lost the lowest weight compared to other used catalysts. The type of coke presented in NiLaMgCa is confirmed in Figure 10. The wasted NiLaMgCa catalyst may have produced the least coke as a result. This is because MgO and CaO absorb CO_2 to generate active carbonate species, which help to gasify coke accumulated on the catalyst by supplying oxygen atoms [66]. Furthermore, NiLaMgCa catalyst with a more significant total number of basic sites also inhibits coke production by accelerating the steam-coke reaction and obstructing the oligomerization phase [67–69]. Fortunately, coke deposition-induced catalyst deactivation is typically reversible, and the coke can be easily removed by air (O_2) oxidation. In most industrial operations, coke is usually burnt off with air to reactivate the used catalyst [70]. An additional element for the suppression of coke is the reaction of $La_2O_2CO_3$ with carbon deposits on the adjacent Ni sites. Thus, it is more stable and active during steam reforming [67,71]. Equations (1) and (2) describe the process underlying the La_2O_3 support ability to inhibit coke [23,67]

$$La_2O_{3(s)} + CO_{2(g)} \leftrightarrow La_2O_2CO_{3(s)} \quad (1)$$

$$La_2O_2CO_{3(s)} + C_{(s)} \leftrightarrow La_2O_{3(s)} + 2CO_{(g)} \quad (2)$$

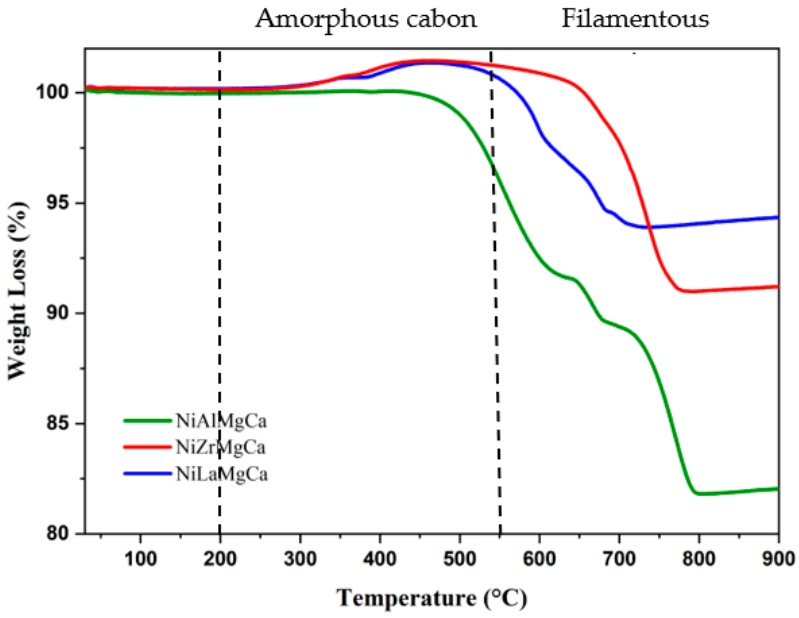

Figure 9. TGA analysis of spent catalyst after 5 h tar steam reforming.

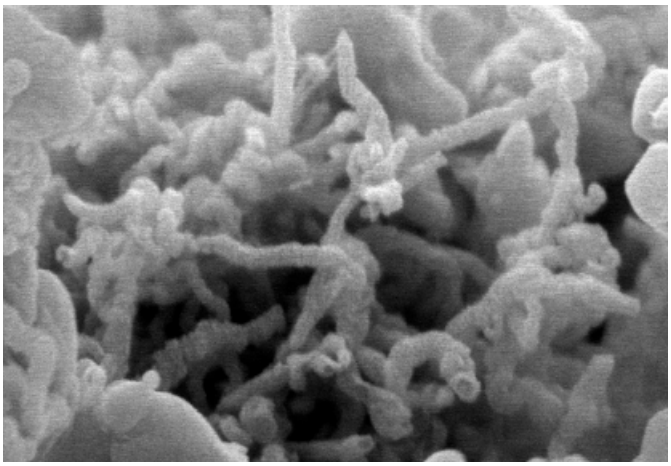

Figure 10. Field emission scanning electron microscopy (FE-SEM) of NiLaMgCa spent catalyst.

Additionally, the Al_2O_3 support strong acidity promotes the dehydrogenation of hydrocarbon into coke over metal phases, which causes the NiAlMgCa catalyst to lose weight. As a result, amorphous coke is deposited on the NiAlMgCa catalyst, which is why the catalytic activity is diminishing [23,72]. While both amorphous and filamentous carbon were seen on the spent NiAlMgCa catalyst, only filamentous carbon was evident on the spent NiLaMgCa catalyst, correlating with the result from the TGA analysis.

The redox capability of the ZrO_2 support is responsible for the weight loss associated with filamentous coke deposited on the NiZrMgCa spent catalysts [20,23,73]. The reactions described in Equations (3) and (4) are redox reactions, which imply that electrons were transferred from one species to another. In steam reformation, the water dissociates on the oxygen vacancies on the support, forming an oxygen lattice. Next, the generated oxygen lattices expanded into the Ni sites to help prevent coke formation [23,74]. Below are the reversible process (Equation (3)) and coke removal reaction (Equation (4)).

$$MO_2 \leftrightarrow MO_{2-x(s)} + O_{2\,(g)} \quad (3)$$

$$C_{(s)} + O_{x(g)} \rightarrow O_{x-1(g)} + CO_{(g)} \quad (4)$$

Additionally, Equation (3) describes the reduction of metal oxide (MO_2) to reduced metal oxide (MO_{2-x}) with the release of oxygen gas (O_2). The transfer of electrons from MO_2 to MO_{2-x} during this reaction further demonstrates the ZrO_2 support has the ability to sustain redox reactions. In Equation (4), O_x is lattice oxygen on the support surface; $C_{(s)}$ is deposited carbon on the catalyst, and O_{x-1} is the reduced site of support. This reaction helps prevent the carbon from depositing on the catalyst surface as coke, which would otherwise reduce its effectiveness. NiLaMgCa is the best catalyst for steam reforming of gasified biomass tar among those tested in this study, according to the findings of characterization, activity testing, and coke formation studies.

3. Materials and Methods

3.1. Catalyst Preparation

Based on the composition shown in Table 4, the co-impregnation process was used to create the 10 wt% Ni-based catalysts. The Ni precursor utilized was nickel nitrate hexahydrate (Ni $(NO_3)26H_2O$) (99%, SigmaAldrich, St. Louis, MO, USA). The catalysts were prepared using g-Al_2O_3 (99.9%, Merck, Rahway, NJ, USA), La_2O_3 (99.9%, SigmaAldrich), and ZrO_2 (99%, SigmaAldrich) as promoters, along with a variety of oxide supports. First, deionized water was combined with the active metal, the oxide support, and the alkaline earth promoter (MgO and CaO). The mixture was constantly agitated at 90 °C until it became a viscous paste. The paste was then completely dried at 110 °C for 12 h After drying, the dried catalyst was calcined at 750 °C for 3 h in the muffle furnace. The catalyst was

then sieved into particles of a size between 34–35 mesh after being pelletized, powdered, and sieved.

Table 4. The weight percentage of each catalyst composition.

Catalyst	Symbol	Ni (wt.%)	MgO (wt.%)	CaO (wt.%)	Al_2O_3 (wt.%)	La_2O_3 (wt.%)	ZrO_2 (wt.%)
Ni/MgO/CaO/Al_2O_3	NiAlMgCa	10	5	5	80	-	-
Ni/MgO/CaO/La_2O_3	NiLaMgCa	10	5	5	-	80	-
Ni/MgO/CaO/ZrO_2	NiZrMgCa	10	5	5	-	-	80
Ni/La_2O_3	NiLa	10	-	-	-	90	-
Ni/Al_2O_3	NiAl	10	-	-	90	-	-
Ni/ZrO_2	NiZr	10	-	-	-	-	90

3.2. Catalyst Characterization

Using a thermogravimetric analyzer, the previously calcined and spent catalysts underwent thermogravimetric analysis (TGA) (Shimadzu TG-50, Kyoto, Japan). Continual airflow was used to heat each catalyst in-situ at a rate of 10 °C/min. It was found that the weight of the catalyst decreased during the temperature range of 30–900 °C. Utilizing a chemisorption analyzer (Micromeriticshemisorb 2720, USA) fitted with a thermal conductivity detector (TCD), temperature-programmed reduction (TPR) analysis was carried out. To get the TPR profile, the calcined catalyst was heated between 250 and 950 °C at a linearly programmed rate of 20 °C/min while flowing at a rate of 20 mL/min of 10 vol% H_2/Ar. Helium (He) flow was supplied to the calcined catalyst at 300 °C for 30 min before the reduction process to rid the catalyst surface of impurities and moisture.

The textural properties of the reduced catalyst were investigated using the Beckman Coulter SA3100 surface area analyzer and N_2 as the adsorptive gas. To clean up impurities from the catalyst surface, the reduced catalyst was degassed at 300 °C with helium (He) flow for 1 h before each analysis. The N_2 adsorption was carried out by liquid N_2 temperature at 77 K throughout a relative pressure between 0–1.

Micromeritics Chemisorb 2720 equipment was used for the analysis of temperature-programmed desorption of carbon dioxide (CO_2-TPD). The reduced catalyst was purged for 30 min at 300 °C in a He flows to eliminate the impurities that had been adsorbed. The excess CO_2 was first eliminated by being purged with He for an additional 30 min after the reduced catalyst had been saturated with 20 mL/min of pure CO_2 at 50 °C. Then, using a linear heating rate of 20 °C/min and a He flow of 20 mL/min, CO_2 desorption was performed from saturation temperature to 900 °C.

The crystalline structure of the reduced catalyst was investigated by X-ray diffraction utilizing a high-resolution X-ray diffractometer (Shimadzu XRD 600, Japan) with a Cu target Ka radiation at 30 kV and 30 mA. The X-ray diffractogram was generated at a scanning speed of 1° and an angle of 2θ ranging from 10 to 80 °C.

3.3. Catalytic Activity Test

The steam-reforming tar model compounds generated during biomass gasification investigated the catalytic performance. The gasified biomass tar model contained 50 wt.% toluene, 30 wt.% naphthalene, 15 wt.% phenol, and 5 wt.% pyrenes. According to the previous study, the components were chosen because they represent the main compounds in gasified biomass [7,75–77]. A fixed bed stainless steel tubular reactor was used for experiments conducted at standard atmospheric pressure (25 cm length, 1.25 cm inner diameter). The experimental setup for catalytic steam reforming is schematically shown in Figure 11.

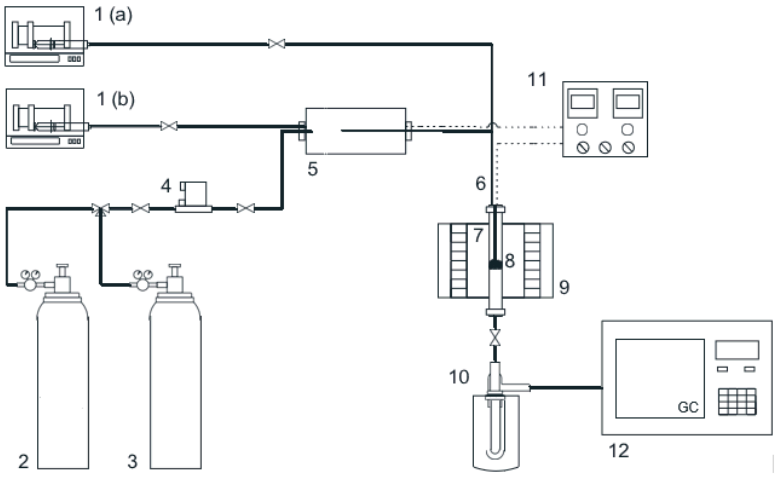

Figure 11. Schematic diagram of steam reforming experimental setup: (1) syringe pump—(a) tar model (b) water; (2) 10% H_2/N_2 cylinder; (3) N_2 cylinder; (4) mass flow controller; (5) turbo vaporizer; (6) K-type thermocouple; (7) stainless steel tubular reactor; (8) catalyst/SiC; (9) furnace; (10) condenser; (11) temperature controller; (12) GC-TCD.

For each test, approximately 0.8 g of catalyst was diluted with silicon carbide (1:2.5 wt ratio) to prevent hot spot formation within the catalyst bed throughout 5 h of reaction [78,79]. The catalyst bed was placed inside the reactor's stainless-steel mesh. The fresh catalyst was reduced at the temperature of 800 °C for 60 min using a stream of 10 vol% H_2/N_2 flowing through the reactor at a 50 mL/min rate. After that, the steam from the reactor was used to steam-reform the chosen gasified biomass tar model compound. Subsequently, a syringe pump was used to directly pump the gasified biomass tar model into the reactor at a rate of about 0.02 mL/min (KD Scientific Series 100, USA). A high-pressure liquid pump supplied 1.66 mL/h of water into the preheater (Lab Alliance Series II).

The feed stream steam-to-carbon (S/C) molar ratio was 1. This is because the stoichiometric value of the S/C molar ratio, which corresponds to the steam reforming of gasified biomass tar, is 0.97. In order to vaporize the water before it enters the reactor, the temperature of the preheater was elevated to 250 °C, to stabilize the temperature inside the reactor. To move the vaporized steam into the reactor, 50 mL/min of N_2 carrier gas was also continually injected into the preheater.

After passing through a condenser containing a mixture of ice and ethanol, the released reaction products were cooled. Using gas chromatography (GC) (Agilent 6890N) and a Carboxen 1010 PLOT capillary GC column (Fused silica 30 m length × 0.53 mm internal diameter, average thickness 30 µm), the gas product was analyzed online. During catalytic steam reforming, numerous parallel reactions are known to take [58,80]. The efficiency of these reactions dictates the selectivity of the overall product. In this experiment, the product selectivity (S_X) was evaluated by calculating the composition of each gaseous product (H_2, CO, CO_2, CH_4) on a dry and N_2-free basis, as indicated in Equation (5). In this study, carbon conversion to gas (Equation (6)) and H_2 yield (Equation (7)) were also considered while evaluating the catalytic activity.

$$S_X(\text{mol}\%) = \frac{\text{mole of X in the product gas}}{\text{total ole of gaseous product}} \times 100 \quad (5)$$

$$\text{Carbon conversion to gas } (\%) = \frac{\text{mole of carbon in product gas}}{\text{mole of carbon in tar fed}} \times 100 \quad (6)$$

$$H_2 \text{ yield } (\%) = \frac{\text{mole of } H_2 \text{ in product gas}}{\text{mole of } H_2 \text{ in tar fed} + \text{mole of } H_2 \text{ in stream}} \times 100 \quad (7)$$

4. Conclusions

Steam reforming of gasified biomass tar is used to convert tar produced from biomass gasification into valuable chemicals and fuels. To improve this process efficiency, the catalyst must have certain properties, such as a strong metal-support interaction, high basicity, and a mesoporous structure. Adding alkaline earth metal promoters, such as MgO and CaO, to the catalyst can improve these properties by strengthening the interaction between the metal and support and increasing the catalyst's basicity. This results in forming a mesoporous structure with an active metallic Ni phase, which is essential for catalytic activity. Among the various catalysts tested, NiLaMgCa was the most effective, exhibiting high catalytic performance and stability in the steam reforming of gasified biomass tar. Furthermore, the buildup of filamentous carbon coke on the spent catalyst did not negatively impact its activity, making NiLaMgCa a suitable catalyst for long-term use in the steam reforming process. NiLaMgCa produced the most carbon-to-gas conversion (86.27 mol%) and H_2 yield (51.58 mol%) after 5 h of reaction compared to other catalysts. Overall, the addition of alkaline earth metal promoters to the catalyst enhances its properties and makes it more effective in the steam reforming of gasified biomass tar.

Author Contributions: A.A., T.A.T.A., W.N. and A.J. designed the experiment; A.A., M.Y.M. and M.L.P.P. performed and collected data; T.A.T.A. supervised and reviewed the final data; A.A., M.Y.M. and M.L.P.P. wrote the original draft preparation; T.A.T.A., W.N., F.M. and M.I. revise, review and edit the paper. All authors have read and agreed to the published version of the manuscript.

Funding: This research was funded by the Malaysia Ministry of Higher Education and Universitat Rovira i Virgili.

Data Availability Statement: The data supporting the findings of the study are available within the article. In addition, data also can be obtained upon request from the corresponding authors.

Acknowledgments: The authors are grateful for the supports given by Universiti Teknologi Malaysia Research University Grant (GUP Tier 1: 20H52) and grant number 4L947. Walid Nabgan is thankful for the support from Universitat Rovira i Virgili under the Maria Zambrano Programme (Reference number: 2021URV-MZ-10), Proyectos de Generación de Conocimiento AEI/MCIN (PID2021-123665OB-I00), and the project reference number of TED2021–129343B-I00.

Conflicts of Interest: The authors declare no conflict of interest.

References

1. Zhai, Y.; Chu, M.; Xie, C.; Huang, F.; Zhang, C.; Zhang, Y.; Liu, H.; Wang, H.; Gao, Y. Synergetic Effect of B and O Dopants for Aerobic Oxidative Coupling of Amines to Imines. *ACS Sustain. Chem. Eng.* **2018**, *6*, 17410–17418. [CrossRef]
2. Cao, L.; Yu, I.K.M.; Xiong, X.; Tsang, D.C.W.; Zhang, S.; Clark, J.H.; Hu, C.; Ng, Y.H.; Shang, J.; Ok, Y.S. Biorenewable hydrogen production through biomass gasification: A review and future prospects. *Env. Res* **2020**, *186*, 109547. [CrossRef]
3. Savuto, E.; Di Carlo, A.; Gallucci, K.; Natali, S.; Bocci, E. Characterization and performance analysis of an innovative Ni/Mayenite catalyst for the steam reforming of raw syngas. *Fuel* **2017**, *194*, 348–356. [CrossRef]
4. Lotfi, S. Technologies for Tar Removal from Biomass-Derived Syngas. *Pet. Petrochem. Eng. J.* **2021**, *5*, 1–35. [CrossRef]
5. Awais, M.; Li, W.; Arshad, A.; Haydar, Z.; Yaqoob, N.; Hussain, S. Evaluating removal of tar contents in syngas produced from downdraft biomass gasification system. *Int. J. Green Energy* **2018**, *15*, 724–731. [CrossRef]
6. Chiodo, V.; Urbani, F.; Zafarana, G.; Prestipino, M.; Galvagno, A.; Maisano, S. Syngas production by catalytic steam gasification of citrus residues. *Int. J. Hydrog. Energy* **2017**, *42*, 28048–28055. [CrossRef]
7. Zeng, R.; Wang, S.; Cai, J.; Kuang, C. A review on Biomass Tar Formation and Catalytic Cracking. *Adv. Eng. Res.* **2018**, *163*, 160–165.
8. Zeng, X.; Ueki, Y.; Yoshiie, R.; Naruse, I.; Wang, F.; Han, Z.; Xu, G. Recent progress in tar removal by char and the applications: A comprehensive analysis. *Carbon Resour. Convers.* **2020**, *3*, 1–18. [CrossRef]
9. Tan, R.S.; Tuan Abdullah, T.A.; Johari, A.; Md Isa, K. Catalytic steam reforming of tar for enhancing hydrogen production from biomass gasification: A review. *Front. Energy* **2020**, *14*, 545–569. [CrossRef]
10. Franchi, G.; Capocelli, M.; De Falco, M.; Piemonte, V.; Barba, D. Hydrogen Production via Steam Reforming: A Critical Analysis of MR and RMM Technologies. *Membranes* **2020**, *10*, 10. [CrossRef]
11. Kalamaras, C.M.; Efstathiou, A.M. Hydrogen Production Technologies: Current State and Future Developments. *Conf. Pap. Energy* **2013**, *2013*, 1–9. [CrossRef]

12. Aljbour, S.; Kawamoto, K. Cerium-Promoted Nickel / Alumina Catalyst for Producer Gas Reforming and Tar Conversion. *J. Ecol. Eng.* **2022**, *23*, 58–66. [CrossRef]
13. Josuinkas, F.M.; Quitete, C.P.B.; Ribeiro, N.F.P.; Souza, M.M.V.M. Steam reforming of model gasification tar compounds over nickel catalysts prepared from hydrotalcite precursors. *Fuel Process. Technol.* **2014**, *121*, 76–82. [CrossRef]
14. Chen, M.; Li, X.; Wang, Y.; Wang, C.; Liang, T.; Zhang, H.; Yang, Z.; Zhou, Z.; Wang, J. Hydrogen generation by steam reforming of tar model compounds using lanthanum modified Ni/sepiolite catalysts. *Energy Convers. Manag.* **2019**, *184*, 315–326. [CrossRef]
15. Savuto, E.; Navarro, R.M.; Mota, N.; Di Carlo, A.; Bocci, E.; Carlini, M.; Fierro, J.L.G. Steam reforming of tar model compounds over Ni/Mayenite catalysts: Effect of Ce addition. *Fuel* **2018**, *224*, 676–686. [CrossRef]
16. Lu, M.; Xiong, Z.; Fang, K.; Li, J.; Li, X.; Li, T. Effect of Promoters on Steam Reforming of Toluene over a Ni-Based Catalyst Supported on Coal Gangue Ash. *ACS Omega* **2020**, *5*, 26335–26346. [CrossRef]
17. Vivanpatarakij, S.; Rulerk, D.; Assabumrungrat, S. Removal of Tar from Biomass Gasification Process by Steam Reforming over Nickel Catalysts. *Chem. Eng. Trans.* **2014**, *37*, 205–210. [CrossRef]
18. Chen, G.; Tao, J.; Liu, C.; Yan, B.; Li, W.; Li, X. Steam reforming of acetic acid using Ni/Al 2 O 3 catalyst: Influence of crystalline phase of Al_2O_3 support. *Int. J. Hydrog. Energy* **2017**, *42*, 20729–20738. [CrossRef]
19. Park, S.Y.; Oh, G.; Kim, K.; Seo, M.W.; Ra, H.W.; Mun, T.Y.; Lee, J.G.; Yoon, S.J. Deactivation characteristics of Ni and Ru catalysts in tar steam reforming. *Renew. Energy* **2017**, *105*, 76–83. [CrossRef]
20. Gao, N.; Salisu, J.; Quan, C.; Williams, P. Modified nickel-based catalysts for improved steam reforming of biomass tar: A critical review. *Renew. Sustain. Energy Rev.* **2021**, *145*, 111023. [CrossRef]
21. Zamzuri, N.H.; Mat, R.; Saidina Amin, N.A.; Talebian-Kiakalaieh, A. Hydrogen production from catalytic steam reforming of glycerol over various supported nickel catalysts. *Int. J. Hydrog. Energy* **2017**, *42*, 9087–9098. [CrossRef]
22. Santamaria, L.; Lopez, G.; Arregi, A.; Amutio, M.; Artetxe, M.; Bilbao, J.; Olazar, M. Influence of the support on Ni catalysts performance in the in-line steam reforming of biomass fast pyrolysis derived volatiles. *Appl. Catal. B Environ.* **2018**, *229*, 105–113. [CrossRef]
23. Tan, R.S.; Abd Jalil, A.; Alir, A.; Mohamad, S.A.; Md Isa, K.; Tuan Abdullah, T.A. Ni-based catalysts for steam reforming of tar model derived from biomass gasification. *E3S Web Conf.* **2019**, *90*, 01015. [CrossRef]
24. Santamaria, L.; Artetxe, M.; Lopez, G.; Cortazar, M.; Amutio, M.; Bilbao, J.; Olazar, M. Effect of CeO_2 and MgO promoters on the performance of a Ni/Al_2O_3 catalyst in the steam reforming of biomass pyrolysis volatiles. *Fuel Process. Technol.* **2020**, *198*, 106223. [CrossRef]
25. Yan, H.; Yao, S.; Zhao, S.; Liu, M.; Zhang, W.; Zhou, X.; Zhang, G.; Jin, X.; Liu, Y.; Feng, X.; et al. Insight into the basic strength-dependent catalytic performance in aqueous phase oxidation of glycerol to glyceric acid. *Chem. Eng. Sci.* **2021**, *230*, 116191. [CrossRef]
26. Sisinni, M.; Di Carlo, A.; Bocci, E.; Micangeli, A.; Naso, V. Hydrogen-Rich Gas Production by Sorption Enhanced Steam Reforming of Woodgas Containing TAR over a Commercial Ni Catalyst and Calcined Dolomite as CO_2 Sorbent. *Energies* **2013**, *6*, 3167–3181. [CrossRef]
27. Clough, P.T.; Boot-Handford, M.E.; Zheng, L.; Zhang, Z.; Fennell, P.S. Hydrogen Production by Sorption Enhanced Steam Reforming (SESR) of Biomass in a Fluidised-Bed Reactor Using Combined Multifunctional Particles. *Materials* **2018**, *11*, 859. [CrossRef]
28. Nogueira, F.G.E.; Assaf, P.G.M.; Carvalho, H.W.P.; Assaf, E.M. Catalytic steam reforming of acetic acid as a model compound of bio-oil. *Appl. Catal. B Environ.* **2014**, *160–161*, 188–199. [CrossRef]
29. Baidya, T.; Cattolica, R.J. Improved catalytic performance of CaO and CeO_2 promoted Ni catalyst on gasifier bed material for tar removal from producer gas. *Appl. Catal. A Gen.* **2015**, *498*, 150–158. [CrossRef]
30. Al-Fatesh, A.S.; Kumar, R.; Fakeeha, A.H.; Kasim, S.O.; Khatri, J.; Ibrahim, A.A.; Arasheed, R.; Alabdulsalam, M.; Lanre, M.S.; Osman, A.I.; et al. Promotional effect of magnesium oxide for a stable nickel-based catalyst in dry reforming of methane. *Sci. Rep.* **2020**, *10*, 13861. [CrossRef]
31. Kim, S.; Chun, D.; Rhim, Y.; Lim, J.; Kim, S.; Choi, H.; Lee, S.; Yoo, J. Catalytic reforming of toluene using a nickel ion-exchanged coal catalyst. *Int. J. Hydrog. Energy* **2015**, *40*, 11855–11862. [CrossRef]
32. Wu, Y.; Pei, C.; Tian, H.; Liu, T.; Zhang, X.; Chen, S.; Xiao, Q.; Wang, X.; Gong, J. Role of Fe Species of Ni-Based Catalysts for Efficient Low-Temperature Ethanol Steam Reforming. *JACS Au* **2021**, *1*, 1459–1470. [CrossRef] [PubMed]
33. Heo, D.H.; Lee, R.; Hwang, J.H.; Sohn, J.M. The effect of addition of Ca, K and Mn over Ni-based catalyst on steam reforming of toluene as model tar compound. *Catal. Today* **2016**, *265*, 95–102. [CrossRef]
34. Mosinska, M.; Maniukiewicz, W.; Szynkowska-Jozwik, M.I.; Mierczynski, P. Influence of NiO/La_2O_3 Catalyst Preparation Method on Its Reactivity in the Oxy-Steam Reforming of LNG Process. *Catalysts* **2021**, *11*, 1174. [CrossRef]
35. Shtyka, O.; Dimitrova, Z.; Ciesielski, R.; Kedziora, A.; Mitukiewicz, G.; Leyko, J.; Maniukewicz, W.; Czylkowska, A.; Maniecki, T. Steam reforming of ethanol for hydrogen production: Influence of catalyst composition (Ni/Al_2O_3, Ni/Al_2O_3–CeO_2, Ni/Al_2O_3–ZnO) and process conditions. *React. Kinet. Mech. Catal.* **2021**, *132*, 907–919. [CrossRef]
36. Wurzler, G.T.; Rabelo-Neto, R.C.; Mattos, L.V.; Fraga, M.A.; Noronha, F.B. Steam reforming of ethanol for hydrogen production over MgO—Supported Ni-based catalysts. *Appl. Catal. A Gen.* **2016**, *518*, 115–128. [CrossRef]
37. Zhao, X.; Xue, Y.; Lu, Z.; Huang, Y.; Guo, C.; Yan, C. Encapsulating Ni/CeO_2-ZrO_2 with SiO_2 layer to improve it catalytic activity for steam reforming of toluene. *Catal. Commun.* **2017**, *101*, 138–141. [CrossRef]

38. Valle, B.; Aramburu, B.; Olazar, M.; Bilbao, J.; Gayubo, A.G. Steam reforming of raw bio-oil over Ni/La_2O_3-αAl_2O_3: Influence of temperature on product yields and catalyst deactivation. *Fuel* **2018**, *216*, 463–474. [CrossRef]
39. Yu, L.; Song, M.; Williams, P.T.; Wei, Y. Alumina-Supported Spinel $NiAl_2O_4$ as a Catalyst for Re-forming Pyrolysis Gas. *Ind. Eng. Chem. Res.* **2019**, *58*, 11770–11778. [CrossRef]
40. Syuhada, A.; Ameen, M.; Sher, F.; Azizan, M.T.; Aqsha, A.; Yusoff, M.H.M.; Ruslan, M.S.H. Effect of Calcium Doping Using Aqueous Phase Reforming of Glycerol over Sonochemically Synthesized Nickel-Based Supported ZrO_2 Catalyst. *Catalysts* **2021**, *11*, 977. [CrossRef]
41. Al-Najar, A.M.A.; Al-Doghachi, F.A.J.; Al-Riyahee, A.A.A.; Taufiq-Yap, Y.H. Effect of La_2O_3 as a Promoter on the Pt,Pd,Ni/MgO Catalyst in Dry Reforming of Methane Reaction. *Catalysts* **2020**, *10*, 750. [CrossRef]
42. Junior, R.B.S.; Rabelo-Neto, R.C.; Gomes, R.S.; Noronha, F.B.; Fréty, R.; Brandão, S.T. Steam reforming of acetic acid over Ni-based catalysts derived from La1−xCaxNiO_3 perovskite type oxides. *Fuel* **2019**, *254*, 115714. [CrossRef]
43. Higo, T.; Saito, H.; Ogo, S.; Sugiura, Y.; Sekine, Y. Promotive effect of Ba addition on the catalytic performance of Ni/$LaAlO_3$ catalysts for steam reforming of toluene. *Appl. Catal. A Gen.* **2017**, *530*, 125–131. [CrossRef]
44. Wu, P.; Tao, Y.; Ling, H.; Chen, Z.; Ding, J.; Zeng, X.; Liao, X.; Stampfl, C.; Huang, J. Cooperation of Ni and CaO at Interface for CO_2 Reforming of CH_4: A Combined Theoretical and Experimental Study. *ACS Catal.* **2019**, *9*, 10060–10069. [CrossRef]
45. Ma, Y.; Liu, J.; Chu, M.; Yue, J.; Cui, Y.; Xu, G. Cooperation Between Active Metal and Basic Support in Ni-Based Catalyst for Low-Temperature CO_2 Methanation. *Catal. Lett.* **2019**, *150*, 1418–1426. [CrossRef]
46. Phuong, P.H.; Loc, L.C.; Cuong, H.T.; Tri, N. Effect of NiO Loading and Thermal Treatment Duration on Performance of Ni/SBA-15 Catalyst in Combined Steam and CO_2 Reforming of CH_4. *Mater. Trans.* **2018**, *59*, 1898–1902. [CrossRef]
47. Ishii, T.; Kyotani, T. Temperature Programmed Desorption. In *Materials Science and Engineering of Carbon*; Butterworth-Heinemann: Oxford, UK, 2016; pp. 287–305.
48. Artetxe, M.; Nahil, M.A.; Olazar, M.; Williams, P.T. Steam reforming of phenol as biomass tar model compound over Ni/Al_2O_3 catalyst. *Fuel* **2017**, *184*, 629–636. [CrossRef]
49. Zhang, Z.; Liu, L.; Shen, B.; Wu, C. Preparation, modification and development of Ni-based catalysts for catalytic reforming of tar produced from biomass gasification. *Renew. Sustain. Energy Rev.* **2018**, *94*, 1086–1109. [CrossRef]
50. Zhang, Z.; Hu, X.; Zhang, L.; Yang, Y.; Li, Q.; Fan, H.; Liu, Q.; Wei, T.; Li, C.-Z. Steam reforming of guaiacol over Ni/Al_2O_3 and Ni/SBA-15: Impacts of support on catalytic behaviors of nickel and properties of coke. *Fuel Process. Technol.* **2019**, *191*, 138–151. [CrossRef]
51. Silveira, E.B.; Rabelo-Neto, R.C.; Noronha, F.B. Steam reforming of toluene, methane and mixtures over Ni/ZrO_2 catalysts. *Catal. Today* **2017**, *289*, 289–301. [CrossRef]
52. Oni, B.A.; Sanni, S.E.; Oyedepo, S.O.; Ibegbu, A.J. Catalytic reforming of tar and volatiles from walnut shell pyrolysis over a novel Ni/olivine/La_2O_3 supported on ZrO_2. *J. Energy Inst.* **2022**, *103*, 33–46. [CrossRef]
53. Gao, X.; Ge, Z.; Zhu, G.; Wang, Z.; Ashok, J.; Kawi, S. Anti-Coking and Anti-Sintering Ni/Al_2O_3 Catalysts in the Dry Reforming of Methane: Recent Progress and Prospects. *Catalysts* **2021**, *11*, 1003. [CrossRef]
54. Kim, H.-J.; Yang, E.-H.; Noh, Y.S.; Hong, G.H.; Park, J.I.; Shin, S.A.; Lee, K.-Y.; Moon, D.J. Studies on the steam CO_2 reforming of methane over ordered mesoporous nickel–magnesium–alumina catalysts. *Res. Chem. Intermed.* **2017**, *44*, 1131–1148. [CrossRef]
55. Oh, G.; Park, S.Y.; Seo, M.W.; Kim, Y.K.; Ra, H.W.; Lee, J.-G.; Yoon, S.J. Ni/Ru–Mn/Al_2O_3 catalysts for steam reforming of toluene as model biomass tar. *Renew. Energy* **2016**, *86*, 841–847. [CrossRef]
56. Lu, M.; Xiong, Z.; Fang, K.; Li, X.; Li, J.; Li, T. Steam reforming of toluene over nickel catalysts supported on coal gangue ash. *Renew. Energy* **2020**, *160*, 385–395. [CrossRef]
57. Nabgan, W.; Tuan Abdullah, T.A.; Mat, R.; Nabgan, B.; Gambo, Y.; Triwahyono, S. Influence of Ni to Co ratio supported on ZrO_2 catalysts in phenol steam reforming for hydrogen production. *Int. J. Hydrog. Energy* **2016**, *41*, 22922–22931. [CrossRef]
58. El-Shafie, M.; Kambara, S.; Hayakawa, Y. Hydrogen Production Technologies Overview. *J. Power Energy Eng.* **2019**, *7*, 107–154. [CrossRef]
59. Quan, C.; Wang, H.; Gao, N. Development of activated biochar supported Ni catalyst for enhancing toluene steam reforming. *Int. J. Energy Res.* **2020**, *44*, 5749–5764. [CrossRef]
60. Chae, H.J.; Kim, J.-H.; Lee, S.C.; Kim, H.-S.; Jo, S.B.; Ryu, J.-H.; Kim, T.Y.; Lee, C.H.; Kim, S.J.; Kang, S.-H.; et al. Catalytic Technologies for CO Hydrogenation for the Production of Light Hydrocarbons and Middle Distillates. *Catalysts* **2020**, *10*, 99. [CrossRef]
61. Łamacz, A. Toluene Steam Reforming over Ni/$CeZrO_2$—The Influence of Steam to Carbon Ratio and Contact Time on the Catalyst Performance and Carbon Deposition. *Catalysts* **2022**, *12*, 219. [CrossRef]
62. Xiaoxu, C.; Duo, W.; Yunquan, L.; Yueyuan, Y.; Shuirong, L.; Yingru, Z. H_2/CO Ratio Adjustment and Tar Removal in Steam Ref orming of Bio-syngas over Nickel-Supported Catalysts. *Acad. J. Agric. Res.* **2016**, *4*, 205–211. [CrossRef]
63. Saad, J.M.; Williams, P.T. Manipulating the H_2/CO ratio from dry reforming of simulated mixed waste plastics by the addition of steam. *Fuel Process. Technol.* **2017**, *156*, 331–338. [CrossRef]
64. Qian, K.; Kumar, A. Catalytic reforming of toluene and naphthalene (model tar) by char supported nickel catalyst. *Fuel* **2017**, *187*, 128–136. [CrossRef]
65. de Castro, T.P.; Silveira, E.B.; Rabelo-Neto, R.C.; Borges, L.E.P.; Noronha, F.B. Study of the performance of Pt/Al_2O_3 and Pt/CeO_2/Al_2O_3 catalysts for steam reforming of toluene, methane and mixtures. *Catal. Today* **2018**, *299*, 251–262. [CrossRef]

66. Tsiotsias, A.I.; Charisiou, N.D.; Yentekakis, I.V.; Goula, M.A. The Role of Alkali and Alkaline Earth Metals in the CO_2 Methanation Reaction and the Combined Capture and Methanation of CO_2. *Catalysts* **2020**, *10*, 812. [CrossRef]
67. Zhang, F.; Wang, M.; Zhu, L.; Wang, S.; Zhou, J.; Luo, Z. A comparative research on the catalytic activity of La_2O_3 and γ-Al_2O_3 supported catalysts for acetic acid steam reforming. *Int. J. Hydrog. Energy* **2017**, *42*, 3667–3675. [CrossRef]
68. Li, C.; Zhang, L.; Gholizadeh, M.; Westernhof, R.; Cui, Z.; Liu, B.; Tang, Y.; Jin, X.; Xu, Z.; Hu, X. Impact of Acidic/Basic Sites of the Catalyst on Properties of the Coke Formed in Pyrolysis of Guaiacol: A Model Compound of the Phenolics in Bio-oil. *Energy Fuels* **2020**, *34*, 11026–11040. [CrossRef]
69. Ochoa, A.; Bilbao, J.; Gayubo, A.G.; Castaño, P. Coke formation and deactivation during catalytic reforming of biomass and waste pyrolysis products: A review. *Renew. Sustain. Energy Rev.* **2020**, *119*, 109600. [CrossRef]
70. Zhou, J.; Zhao, J.; Zhang, J.; Zhang, T.; Ye, M.; Liu, Z. Regeneration of catalysts deactivated by coke deposition: A review. *Chin. J. Catal.* **2020**, *41*, 1048–1061. [CrossRef]
71. Palma, V.; Ruocco, C.; Cortese, M.; Martino, M. Bioalcohol Reforming: An Overview of the Recent Advances for the Enhancement of Catalyst Stability. *Catalysts* **2020**, *10*, 665. [CrossRef]
72. Jang, E.J.; Lee, J.; Jeong, H.Y.; Kwak, J.H. Controlling the acid-base properties of alumina for stable PtSn-based propane dehydrogenation catalysts. *Appl. Catal. A Gen.* **2019**, *572*, 1–8. [CrossRef]
73. Kauppi, E.I.; Honkala, K.; Krause, A.O.I.; Kanervo, J.M.; Lefferts, L. ZrO_2 Acting as a Redox Catalyst. *Top. Catal.* **2016**, *59*, 823–832. [CrossRef]
74. Sumarasingha, W.; Supasitmongkol, S.; Phongaksorn, M. The Effect of ZrO_2 as Different Components of Ni-Based Catalysts for CO_2 Reforming of Methane and Combined Steam and CO_2 Reforming of Methane on Catalytic Performance with Coke Formation. *Catalysts* **2021**, *11*, 984. [CrossRef]
75. Rakesh, N.; Dasappa, S. A critical assessment of tar generated during biomass gasification—Formation, evaluation, issues and mitigation strategies. *Renew. Sustain. Energy Rev.* **2018**, *91*, 1045–1064. [CrossRef]
76. Madav, V.; Das, D.; Kumar, M.; Surwade, M.; Parikh, P.P.; Sethi, V. Studies for removal of tar from producer gas in small scale biomass gasifiers using biodiesel. *Biomass Bioenergy* **2019**, *123*, 123–133. [CrossRef]
77. Singh, R.N.; Singh, S.P.; Balwanshi, J.B. Tar removal producer gas: A review. *Res. J. Eng. Sci.* **2014**, *3*, 16–22.
78. Kulkarni, S.R.; Velisoju, V.K.; Tavares, F.; Dikhtiarenko, A.; Gascon, J.; Castaño, P. Silicon carbide in catalysis: From inert bed filler to catalytic support and multifunctional material. *Catal. Rev.* **2022**, *65*, 174–237. [CrossRef]
79. Duong-Viet, C.; Ba, H.; El-Berrichi, Z.; Nhut, J.-M.; Ledoux, M.J.; Liu, Y.; Pham-Huu, C. Silicon carbide foam as a porous support platform for catalytic applications. *New J. Chem.* **2016**, *40*, 4285–4299. [CrossRef]
80. Zhu, H.L.; Pastor-Pérez, L.; Millan, M. Catalytic Steam Reforming of Toluene: Understanding the Influence of the Main Reaction Parameters over a Reference Catalyst. *Energies* **2020**, *13*, 813. [CrossRef]